THE JOURNAL OF BIOLOGICAL CHEMISTRY VOL. 281, NO. 33, pp. 23990–23998, August 18, 2006

Crystal Structures of Chloroperoxidase with Its Bound Substrates and Complexed with Formate, Acetate, and Nitrate*

Received for publication, April 3, 2006, and in revised form, May 26, 2006 Published, JBC Papers in Press, June 20, 2006, DOI 10.1074/jbc.M603166200

Karin Kühnel[‡], **Wulf Blankenfeldt**[‡§], **James Terner**[¶], **and Ilme Schlichting**[‡1]

From the [‡]*Abteilung Biomolekulare Mechanismen, Max-Planck-Institut für Medizinische Forschung, Jahnstrasse 29, 69120 Heidelberg, Germany, the* [§]*Abteilung Physikalische Biochemie, Max-Planck-Institut für Molekulare Physiologie, 44227 Dortmund, Germany, and the* [¶]*Department of Chemistry, Virginia Commonwealth University, Richmond, Virginia 23284-2006*

Chloroperoxidase (CPO) is a heme-thiolate enzyme that catalyzes hydrogen peroxide-dependent halogenation reactions. Structural data on substrate binding have not been available so far. CPO was therefore crystallized in the presence of iodide or bromide. One halide binding site was identified at the surface near a narrow channel that connects the surface with the heme. Two other halide binding sites were identified within and at the other end of this channel. Together, these sites suggest a pathway for access of halide anions to the active site. The structure of CPO complexed with its natural substrate cyclopentanedione was determined at a resolution of 1.8 Å. This is the first example of a CPO structure with a bound organic substrate. In addition, structures of CPO bound with nitrate, acetate, and formate and of a ternary complex with dimethylsulfoxide (Me_2SO) and cyanide were determined. These structures have implications for the mechanism of compound I formation. Before binding to the heme, the incoming hydrogen peroxide first interacts with Glu-183. The deprotonated Glu-183 abstracts a proton from hydrogen peroxide. The hydroperoxo-anion then binds at the heme, yielding compound 0. Glu-183 protonates the distal oxygen of compound 0, water is released, and compound I is formed.

Chloroperoxidase (CPO)[2] is a 42-kDa heme-containing glycoprotein that is secreted by the fungus *Caldariomyces fumago*. The enzyme catalyzes the hydrogen peroxide-dependent chlorination of cyclopentanedione during the biosynthesis of the antibiotic caldarioymcin (1, 2). Additionally, CPO catalyzes the iodination and bromination of a wide range of substrates (3–5). Besides performing H_2O_2-dependent halogenation reactions, the enzyme catalyzes dehydrogenation reactions (6). These reactions can be performed in a stereoselective manner by CPO (7). CPO also functions as a catalase, facilitating the decomposition of hydrogen peroxide to oxygen and water (6). Furthermore, CPO catalyzes P450-like oxygen insertion reactions (8). Of particular interest for commercial applications is the enantioselective formation of epoxides from alkenes (9, 10), because CPO utilizes H_2O_2, whereas P450 enzymes depend on both molecular oxygen and electron transfer proteins. The capability of CPO to perform these diverse reactions makes it one of the most versatile of all known heme proteins. Structurally, CPO is unique, but it shares features with both peroxidases and P450 enzymes (11). As in cytochrome P450 enzymes, the proximal heme ligand of CPO is a cysteine (Cys-29), but similar to peroxidases, the distal side of the heme in CPO is polar. However, unlike other peroxidases, the normally conserved distal arginine is lacking in CPO and the catalytic acid base of CPO is a glutamic acid (Glu-183) and not a histidine. When Glu-183 is mutated to a histidine, the chlorination activity is reduced by 85%, which indicates the importance of this acidic residue for the catalytic activity of CPO (12). CPO is reactive at low pH with an optimum at pH 2.8 (1), which is likely due to the high redox potential required to oxidize a chloride anion, and therefore a glutamic acid residue instead of a histidine is used as a catalytic acid base. The crystal structure of CPO in the ferric ground state was determined more than 10 years ago by the group of Thomas Poulos (11). On the distal side of the heme, a water molecule is located 3.4 Å away from the iron. This water is displaced by the incoming H_2O_2. It is generally assumed that Glu-183 abstracts a proton from the hydrogen peroxide bound to heme, yielding a short-lived peroxo-anion species (compound 0) (13). In the next step Glu-183 is expected to protonate the terminal oxygen to facilitate the heterolytic cleavage of the O–O bond. Subsequently, water is released and compound I, the oxoferryl(IV) porphyrin π cation radical, is formed. Compound I can oxidize a chloride anion and has been proposed to form an Fe(III)-hypohalite intermediate (14). Such a species has been detected spectroscopically at pH 4.4 (13). However, it has not yet been entirely resolved whether this hypohalite intermediate directly chlorinates the organic substrate (15), or if HOCl is released upon protonation of the intermediate, and free HOCl or Cl_2 perform the chlorination reactions (16). Because CPO shows only low substrate specificity and chlorinates a wide range of substrates non-stereospecifically (17), it might indeed be that free HOCl or Cl_2 perform these reactions in

* This work was supported by the Peter und Traudl Engelhorn-Stiftung (to K. K.), the Deutsche Forschungsgemeinschaft (to I. S.), and National Institutes of Health Grant GM57042 (to J. T.). Diffraction data were collected at the Swiss Light Source, Paul Scherrer Institute, Villigen, Switzerland and the European Synchrotron Radiation Facility Grenoble, France. The costs of publication of this article were defrayed in part by the payment of page charges. This article must therefore be hereby marked "*advertisement*" in accordance with 18 U.S.C. Section 1734 solely to indicate this fact.

The atomic coordinates and structure factors (codes 2civ, 2civ, 2cix, 2ciy, 2ciz, 2cj0, 2cj1, and 2cj2) have been deposited in the Protein Data Bank, Research Collaboratory for Structural Bioinformatics, Rutgers University, New Brunswick, NJ (http://www.rcsb.org/).

[1] To whom correspondence should be addressed. Tel.: 49-6221-486-500; Fax: 49-6221-486-585; E-mail: ilme.schlichting@mpimf-heidelberg.mpg.de.

[2] The abbreviations used are: CPO, chloroperoxidase; CPD, cyclopentanedione; PEG, polyethylene glycol.

solution. In contrast, it has been reported that glycals (18) and steroids (19, 20) are stereospecifically halogenated, indicating that there must be an interaction between the organic substrate and CPO. Binding of organic substrates at the active site is also supported by the observation that epoxidation and sulfoxidation reactions (21) are catalyzed stereospecifically. Binding of the substrate cyclopentanedione (CPD) to CPO has been shown by NMR titration experiments (22).

The structures of CPO bound with small diatomic or triatomic ligands, *e.g.* carbon monoxide, nitric oxide, cyanide, and thiocyanate have been determined, but so far the soaking of organic substrates into CPO crystals has been unsuccessful (23). Therefore information on the structural basis of substrate binding and specificity has been limited.

Here we present crystal structures of CPO bound to its substrate CPD and of a ternary complex of the enzyme with cyanide and Me_2SO. We co-crystallized CPO with either bromide or iodide and could identify several binding sites, which suggest a pathway for halide access to the heme. Also described are the structures of CPO complexed with acetate, nitrate, and formate, which have been shown to bind to the enzyme (24). The implications of these structures for the mechanism of compound I formation are discussed.

EXPERIMENTAL PROCEDURES

Co-crystallization with Halides—CPO was expressed and purified as described previously (25). Crystals were grown by the hanging drop method at 20 °C. 1 μl of 15 mg/ml CPO in 5 mM sodium acetate buffer, pH 3.8, was mixed with 1 μl of the reservoir solution. The reservoir solution for the iodide crystals contained 50 mM NaI, 20% PEG 3350, and 0.1 M sodium citrate at pH 3.6, similar to previously published crystallization conditions (11). Rod-like crystals grew within a few days. CPO crystals were flash-cooled in liquid nitrogen after transfer into 10% (w/v) sucrose, 10% (w/v) xylitol, 50 mM NaI, 20% PEG 3350, and 0.1 M sodium citrate at pH 3.6. Bromide-containing crystals were grown in a similar fashion as the iodide crystals in a reservoir solution containing 0.1 M KBr, 22% PEG 3000, and 0.1 M sodium citrate at pH 3.6. The cryoprotectant solution for the bromide crystals consisted of mother liquor supplemented with 10% (w/v) sucrose and 10% (w/v) xylitol.

Complexes with Cyclopentanedione and Me_2SO—A 2 M CPD stock solution was prepared in Me_2SO. Crystals grown in mother liquor containing KBr were transferred into a soaking solution containing 200 mM CPD, 10% Me_2SO, 50 mM KBr, 22% PEG 3000, and 0.1 M citrate at pH 3.6 and were incubated for 15 min at 20 °C. Crystals were then moved into the soaking solution supplemented with 15% ethylene glycol for cryoprotection and flash-cooled in liquid nitrogen. A CPD-cyanide ternary complex was attempted by first soaking the crystals in 50 mM KCN, 50 mM KBr, 22% PEG 3000, and 0.1 M sodium citrate at pH 6 for 5 min at 20 °C. Crystals were then transferred to a solution containing 50 mM KCN, 200 mM CPD, 10% Me_2SO, 50 mM KBr, 22% PEG 3000, and 0.1 M sodium citrate at pH 6 for 10 min at 20 °C. Crystals were subsequently moved into a cryoprotectant containing 15% ethylene glycol, 50 mM KCN, 200 mM CPD, 10% Me_2SO, 50 mM KBr, 22% PEG 3000, and 0.1 M sodium citrate at pH 6 and cryogenically cooled.

Nitrate-, Formate-, and Acetate-bound Complexes—The reservoir solution for the nitrate complex contained 50 mM $Mg(NO_3)_2$, 20% PEG 3000, and 0.1 M citrate at pH 3.6. The cryoprotectant solution contained 30% ethylene glycol, 50 mM $Mg(NO_3)_2$, 20% PEG 3000, and 0.1 M citrate at pH 3.6. The CPO formate crystals were grown in a solution containing 100 mM sodium formate, 24% PEG 3000, and 0.1 M citrate at pH 3.6. The acetate complex was prepared by soaking CPO crystals grown in the presence of 50 mM KBr in a solution containing 300 mM acetic acid, 50 mM KBr, 22% PEG 3000, and 0.1 M citrate at pH 2 for 10 min at 20 °C. Crystals were transferred into a cryoprotectant consisting of mother liquor supplemented with either 15% ethylene glycol, or 10% (w/v) xylitol and 10% (w/v) sucrose, and then cryo-cooled in liquid nitrogen.

Data Collection and Structure Solution—Diffraction data of cryo-cooled crystals were collected at 100 K with a Nonius FR591 rotating anode or at synchrotrons at beamlines X06SA, X10SA (Swiss Light Source, Villigen, Switzerland), and ID 14-4 (European Synchrotron Radiation Facility, Grenoble, France). Data were processed with the XDS software package (26) (see Table 1). Structures were determined by molecular replacement with Amore (27) using the previously published CPO structure (pdb accession code: 1cpo) (11) as a search model. The graphics program O was used for manual rebuilding of the model (28). Refinement was carried out initially with CNS (29) and at later stages with Refmac5 (30). Waters were picked with ArpWarp (31). Figures were prepared with Molscript (32), Bobscript (33), and Pymol.[3]

RESULTS

Halide-bound Structures—CPO catalyzes chlorination, bromination, and iodination reactions. CPO has been previously crystallized in the presence of 300 mM NaCl, but despite the high chloride concentration and good resolution of the data (1.9 Å) no chloride ions were included in the model (11). We attempted to identify halide binding sites by making use of the anomalous signals of bromine and iodine (Fig. 1*A*). This approach was not feasible with chlorine, because the K-edge of this element is at 4.39 Å. Therefore, CPO was crystallized in the presence of either NaI or KBr. A 1.7-Å resolution data set of a CPO-iodide crystal was collected in-house (Table 1). Iodine shows a strong anomalous signal at the copper Kα wavelength. An anomalous bromine data set (K-edge) was measured at the synchrotron. Using anomalous difference electron density maps, a bromide/iodide binding site (I/Br1) was identified at the surface of CPO (Fig. 1, *A* and *B*). This binding site has occupancies of 60% for bromide and 30% for iodide and likely serves as a docking site for halide anions. The anion binds in a dent on the surface and is stabilized by a hydrogen bond with the backbone amide of Ala-265, and by participation in a water network. This site is close to a narrow channel connecting the protein surface with the heme. In addition, there is a second channel with a larger diameter connecting the surface and active site but no halides bound in proximity to this channel.

8 Å away from the docking site I/Br1, a second binding site (I/Br2) is located within the narrow channel (Fig. 1*B*). The

[3] W. L. DeLano (2002) Pymol, DeLano Scientific, San Carlos CA.

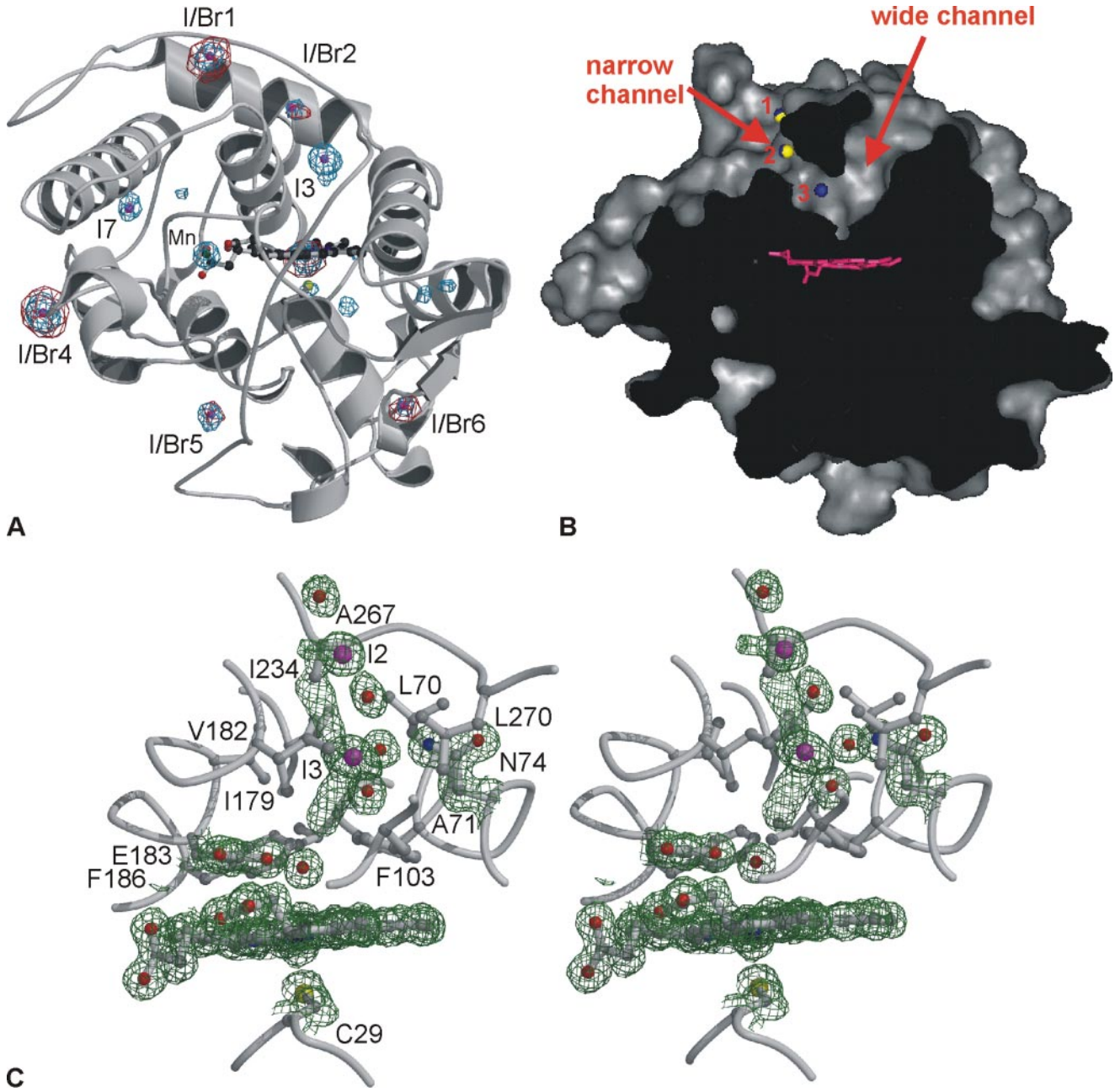

FIGURE 1. **Binding of halides to CPO.** *A*, anomalous difference maps calculated from iodide (*blue*) and bromide data (*red*) shown at $+4\sigma$ (iodine) and $+3.5\ \sigma$ (bromide) contour levels. Besides the halide binding sites, the heme iron and manganese ion (*green*) located next to the heme also show anomalous signals. The weaker peaks visible in the iodide anomalous difference map are caused by the sulfur atoms of methionines and cysteines. *B*, slice through a surface representation of CPO (including sugars attached to the protein). The two channels leading to the active site are marked by *arrows*, and the heme is shown in *magenta*. The halide binding site 2 (*yellow sphere*, bromide; *blue*, iodide) is located within the narrow channel and the iodide specific binding site 3 at the end of the channel implicating a pathway for halide access from the surface (*site 1*) to the heme though this narrow channel. *C*, stereoview of the active site with bound iodide. The 1.15-Å electron density map (sigmaA-weighted $2mF_o - DF_c$ map with 1σ contour level) is shown for selected residues, including the water funnel and the iodide (*magenta*).

anions bound at this position do not interact directly with the protein but instead participate in a water network, which might explain the low occupancy observed for this site (20% for iodide and 30% for bromide). The channel has a radius of ~2 Å. A third binding site specific for iodide (I3), occupancy 40%, is present at the end of the channel above the heme (Fig. 1, *A–C*). This site is located 6 Å from halide binding site 2 and 8.8 Å from the heme iron. The amide group of Asn-74 forms a hydrogen bond with the iodide (distance, 3.5 Å). The iodide also forms hydrogen bonds with water molecules, which are present in the middle of the wider channel (Fig. 1*C*). The other neighbors of I3 are hydrophobic with distances of ~4 Å to the side chains of residues Leu-70, Phe-103, Ile-179, and Ala-267, respectively. These three sites suggest a pathway for halide access to the heme through the narrow channel. Although no binding sites of halides were observed in the wide channel, we cannot exclude diffusion of halide anions through the wider channel to the heme.

Soaking crystals with high concentrations of bromide or iodide can be used to prepare heavy atom derivatives for phas-

TABLE 1

Crystallographic data collection and refinement statistics

CPO complexes	Iodide		Bromide	CPD	Me_2SO/cyanide	Acetate	Nitrate	Formate	
	Low res.	High res.						Ethylene glycol	Sugar
Data collection									
PDB accession code		2ciw	2civ	2cix	2ciy	2ciz	2cj0	2cj1	2cj2
Space group	$C222_1$	$C222_1$	$C222_1$	$C222_1$	$C222_1$	$C222_1$	$C222_1$	$C222_1$	$C222_1$
Unit cell dimensions *a*, *b*, *c* (Å)	57.6, 151.2, 100.6	57.7, 151.4, 100.7	57.5, 150.8, 100.4	57.4, 150.4, 99.6	58.2, 151.0, 101.1	57.5, 150.8, 100.4	56.9, 150.6, 100.6	58.3, 150.3, 99.7	57.9, 150.6, 100.3
Beamline/x-ray source	Nonius, FR591	ESRF, ID 14-4	SLS, X10SA	ESRF, ID 14-4	SLS, X10SA	SLS, X10SA	SLS, X06SA	SLS, X06SA	SLS, X10SA
Wavelength (Å)	1.542	0.920	0.918	1.040	1.008	0.925	0.902	1.006	1.069
Resolution of data (Å) (high res. bin)	20–1.7 (1.74–1.70)	20–1.15 (1.18–1.15)	20–1.8 (1.85–1.80)	20–1.8 (1.85–1.80)	20–1.7 (1.74–1.70)	20–1.3 (1.33–1.30)	20–1.75 (1.80–1.75)	20–1.7 (1.74–1.70)	20–1.6 (1.64–1.60)
No. of observations	192,699	658,979	207,470	197,234	161,308	394,415	299,698	118,807	172,149
Unique reflections	90,232	155,718	77,290	39,927	46,800	104,573	43,689	47,188	56,733
Completeness total (high) (%)	96.6 (76.5)	97.8 (94.3)	98.4 (94.0)	97.1 (92.5)	92.5 (64.2)	94.7 (76.9)	98.0 (94.8)	93.9 (87.0)	94.3 (76.1)
$I/\sigma I$ total (high)	15.5 (5.1)	10.6 (3.2)	14.4 (8.2)	16.3 (3.8)	15.5 (3.2)	9.9 (2.9)	18.0 (5.6)	9.9 (2.9)	12.9 (2.5)
R_{sym} total (high) %	3.3 (16.1)	6.0 (39.3)	5.7 (10.5)	13.9 (41.1)	5.7 (33.7)	9.2 (33.2)	6.7 (36.2)	7.7 (40.9)	5.9 (38.8)
Wilson *B*-factor (Å^2)	13.8	15.9	20.5	28.1	23.4	17.9	25.9	25.8	23.1
Refinement									
R_{work}/R_{free} (%)	16.9/19.2	14.9/17.1	15.9/18.4	17.8/21.7	17.9/20.4	14.8/17.0	17.3/20.7	18.9/22.9	17.9/20.4
Protein residues (no. of atoms)	298 (2316)	298 (2316)	298 (2316)	298 (2316)	298 (2316)	298 (2316)	298 (2316)	298 (2316)	298 (2316)
Sugar residues (no. of atoms)	17 (199)	18 (210)	17 (199)	17 (213)	17 (213)	17 (202)	19 (224)	18 (210)	18 (213)
Water	470	608	426	345	398	579	359	349	474
Ligands (total atoms)	7 I, heme (43), 1 Mn (1)	7 I, heme (43), 1 Mn (1)	5 Br, heme (43), 1 Mn (1)	CPD (7), heme (43), 1 Mn (1), 3 Br (3), 1 ethylene glycol (4)	1 CN (2), 1 Me_2SO (4), heme (43), 1 Mn (1), 2 Br (2), 3 ethylene glycol (12)	2 acetate (8), heme (43), 1 Mn (1), 3 Br, 2 ethylene glycol (8)	1 nitrate (4), heme (43), 1 Mn (1), 3 ethylene glycol (12)	1 formate (3), heme (43), 1 Mn (1), 3 ethylene glycol (12)	1 formate (3), heme (43), 1 Mn (1)
Overall *B*-factor (Å^2)	17.7	12.7	15.9	22.8	17.4	12.2	21.4	21.7	19.3
Root mean square deviations									
Bond length (Å)	0.012	0.013	0.011	0.013	0.013	0.012	0.012	0.014	0.011
Bond angles (°)	1.37	1.53	1.33	1.51	1.37	1.50	1.44	1.45	1.34

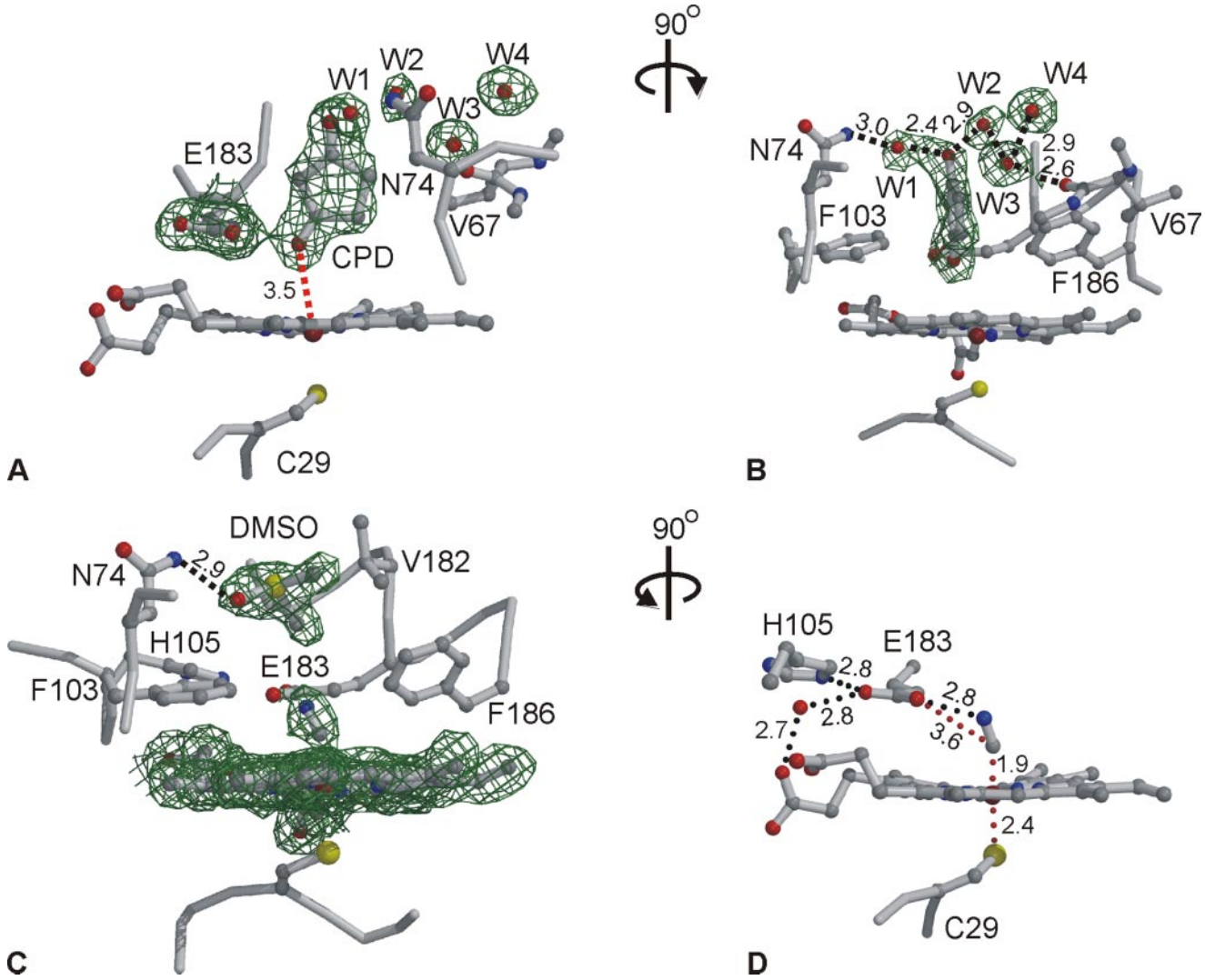

FIGURE 2. **CPO complexed with cyclopentanedione and a ternary complex with cyanide and Me_2SO.** *A* and *B*, cyclopentanedione bound at the active site is shown in two orientations. The final electron densities are shown (sigmaA-weighted $2mF_o - DF_c$ map, 1σ contour level). *C*, CPO complexed with Me_2SO and cyanide. *D*, close up of the active site with bound cyanide. Distances in Å are shown for hydrogen bonds (*black*) and selected interatomic distances (*red*).

ing. The anions mainly bind in the ordered solvent region at the protein surface (35). Also in CPO, four additional halide binding sites, showing different occupancies, are located at the surface of the molecule. At these sites, the anions replaced water molecules from the solvent shell. The halide anions form hydrogen bonds with side chains and amides of the protein backbone, and form ion pairs with positively charged basic residues. The iodide and bromide at binding site 4 also interact with a symmetry-related CPO molecule. These binding sites on the surface are far away from the channels leading to the heme and are unlikely to be of catalytic relevance.

We obtained a 1.15-Å resolution data set from an exceptionally well diffracting CPO-iodide crystal at the synchrotron. The high resolution structure gives detailed insight into the location of water molecules at the active site (Fig. 1*C*). Near the heme, the wider channel is lined by mainly hydrophobic side chains with the exception of Glu-183 and Asn-74. A narrow water funnel is present in the center of this channel. The water molecules are arranged like pearls on a string within this funnel, although not at fixed positions. The side chains of Phe-186 and Phe-103 are located almost parallel atop of the heme plane and shield the active site from solvent. The distance between Phe-186 and Phe-103 is 6.2 Å. A water molecule is ~3.5 Å away from both aromatic side chains and is stabilized at this position by a hydrogen bond with Glu-183. The distance between the iron and this water is 3.5 Å.

Complexes of CPO with Organic Substrates—CPO has been proposed to catalyze the chlorination of CPD during biosynthesis of caldariomycin (1, 2). NMR titration experiments showed that CPO binds CPD with only low affinity (K_d = 33 mM) (22), which might explain why diffusing organic substrates into CPO crystals was previously unsuccessful (23). Because CPD binds only weakly, crystals were soaked in solutions containing very high concentrations of CPD (200 mM). A data set was collected to a resolution of 1.8 Å. CPD binds above the heme and is sandwiched between Phe-103 and Phe-186, with a distance of ~3.5 Å to both aromatic side chains (Fig. 2, *A* and *B*). The substrate displaces the heme water, with one carbonyl oxygen of CPD adopting the position of the water. The distance between this carbonyl oxygen and Glu-183 is 2.5 Å. The second

carbonyl oxygen of CPD forms hydrogen bonds with two water molecules, one of which in turn forms a hydrogen bond with Asn-74, whereas the former participates in a network of water molecules (Fig. 2*B*). Only a small conformational change is observed in the protein upon substrate binding; the side chain of Phe-103 moves 0.5 Å away from the active site for steric reasons.

The position of the bound substrate observed here seems unproductive with respect to the chlorination reaction for two reasons. First, the methylene group, which becomes halogenated, is in an unfavorable orientation. It points away from the active site, and the distance between the carbon and the iron is 5.8 Å. Second, the molecule binds too close to the active site, which would not permit formation of the hypohalite intermediate from hydrogen peroxide and chloride, because the distance between the CPD carbonyl oxygen and iron is only 3.4 Å. Nevertheless, the CPD-bound structure explains the results of NMR titration experiments (22). CPD binds with only low affinity (K_d = 33 mM), but when iodide was present the affinity between CPO and CPD decreased even further (K_d = 123 mM). When superimposing the iodide and the CPD-bound structure it became clear that CPD clashes with the iodide-specific binding site, because the distance between the second carbonyl oxygen and the iodide is only 1.9 Å. The dissociation constant of CPD binding in the presence of NaCl is 31 mM, very similar to the value observed in the absence of halides (22), indicating that chloride does not bind at this site and further supports the idea that this binding site is specific for iodide.

To force CPD to bind at a different, catalytically more sensible site, we tried to block the above described binding site by soaking the crystals first in cyanide, which coordinates to the iron, and then transfer the crystals into a CPD-containing solution. Diffraction data were collected to a resolution of 1.7 Å. A cyanide molecule bound at the heme iron is visible in the electron density map (Fig. 2*C*). The diatomic ligand binds in a slightly bent orientation with an Fe–C–N angle of 156°. The distance between the cyanide carbon and the iron is 1.9 Å (Fig. 2*D*). This differs significantly from the previously reported value of 2.6 Å for a CPO-cyanide complex (23). The shorter distance is in agreement with previously reported values (36, 37).

However, no CPD was observed in the CPO-cyanide complex. Instead, previously unobserved density was visible at the iodide binding site (Fig. 2*C*). This density corresponds to Me_2SO, which was used to prepare the CPD stock solution. The final Me_2SO concentration in the soaking solutions was 10% (v/v). It has been observed earlier that Me_2SO is also a substrate of CPO (38). CPO reacts with Me_2SO and H_2O_2 in the absence of halides and forms dimethyl sulfone. When the reaction is carried out with bromide or chloride, dimethyl sulfone remains the major product and ~1% of either bromodimethyl sulfoxide or chlorodimethyl sulfone are formed (38).

The sulfoxide oxygen and the side-chain amide group of Asn-74 form a hydrogen bond (distance 2.9 Å). The Me_2SO molecule is not in a favorable orientation for the sulfur to react with the compound I intermediate to form dimethyl sulfone, because the sulfur faces away from the active site. Also, the distance between sulfur and iron is too large (7.8 Å) for a direct interaction with a reactive oxygen species. Nevertheless, it is very likely that Me_2SO binds transiently at this site when it diffuses through the channel to the heme. The distance between the methyl group of Me_2SO and the nitrogen of the cyanide (3.3 Å) would permit a direct halogenation of Me_2SO by the hypohalite iron intermediate.

CPO Complexed with Acetate, Nitrate, and Formate—Nitrate, acetate, and formate all bind to the active site of CPO. The dissociation constants have been previously determined spectroscopically. The values reported at pH 3 are 0.55 mM for nitrate, 93 mM for acetate, and 0.135 mM for formate, respectively (24).

At low pH, both nitrate and acetate bind at the distal site of the heme and are sandwiched between Phe-103 and Phe-186 (Fig. 3*B*). The acetate adopts two conformations (Fig. 3, *A* and *B*). In its first conformation, the acetate and also the nitrate are located in a similar orientation perpendicular to the heme plane but do not bind straight above the iron, because that would cause steric clashes with Phe-186 (Fig. 3, *A*–*C*). This aromatic residue also causes acetate to bind in a tilted orientation toward the heme in its second conformation. The angle between the planes spanned by the heme and the acetate molecule is ~60°. The distance between the acetate oxygen and the iron is only 2.4 Å compared with 3.5 Å in the conformation further away, thus heme and the "closer" acetate can interact. The two conformations of acetate observed in the high resolution crystal structure (1.3 Å) are consistent with spectroscopic data showing that the CPO-acetate complex has a mixed spin state (24). Also, the long distance of 3.5 Å between the nitrate oxygen and heme iron agrees with the observation that the nitrate-CPO complex adopts a high spin state (24). In the CPO-acetate structure, the aromatic side chain of Phe-103 moves 0.5 Å away from the active site, very similar to the CPD-complexed structure but unlike the nitrate-bound structure. The oxygen atoms of both nitrate and the first conformation of the acetate occupy the same position as the ferric water and form hydrogen bonds with Glu-183. In the nitrate structure an ethylene glycol molecule is bound above the ligand (Fig. 3*C*), which was added as a cryoprotectant. This ethylene glycol forms hydrogen bonds with both nitrate and Asn-74.

Glu-183 needs to be protonated to form a hydrogen bond with the nitrate anion. CPO shows a much lower affinity toward acetate and formate at pH 6 compared with pH 3 (24). At pH 6 Glu-183, acetate and formate are deprotonated and negative charges on both the catalytic residue and the ligands are repulsive. At lower pH weaker acidic ligands than glutamic acid (pK_a ~ 4.1) are protonated, and the ligands can form hydrogen bonds with the deprotonated Glu-183; therefore, the affinity is significantly increased in comparison to higher pH values.

The structures of CPO complexed with formate were determined in the presence of either ethylene glycol or xylitol/sucrose cryoprotectants. The formate binds in a single conformation parallel to the heme plane in the ethylene glycol structure (1.7-Å resolution, Fig. 3*D*). This is in contrast to the situation in horseradish peroxidase, where the formate adopts a position perpendicular to the heme and the proximal oxygen atom of formate directly interacts with the iron (39). In contrast to the acetate, nitrate, and CPD-bound CPO structures, the oxygen

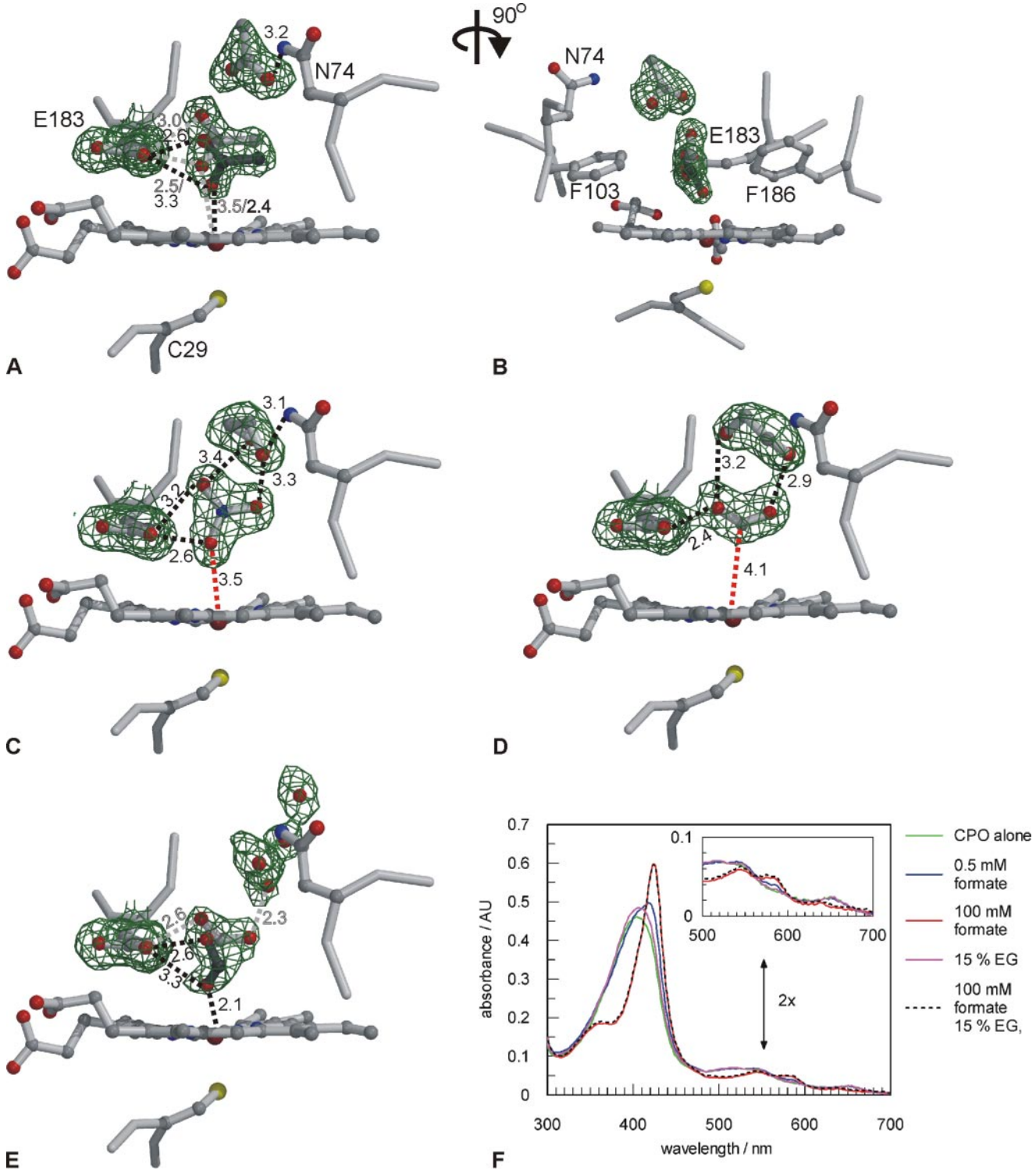

FIGURE 3. **Complexes of CPO with acetate, nitrate, and formate.** *A* and *B*, acetate binds in two conformations at the active site (shown in *light* and *dark gray*). A second acetate molecule binds in the solvent channel near the iodide binding site. Two orientations rotated by 90° are shown. Final sigmaA-weighted $2mF_o - DF_c$ maps are shown with a contour level of 1σ. *C*, CPO complexed with nitrate. An ethylene glycol molecule used as cryoprotectant is located above the nitrate. The ethylene glycol binds at the iodide specific binding site 3 and forms a hydrogen bond with Asn-74. *D*, complex of CPO with formate in the presence of ethylene glycol. A formate molecule is bound at the active site and forms hydrogen bonds with an ethylene glycol molecule. *E*, CPO-formate complex with a xylitol and sucrose-containing cryoprotectant. The formate binds in two orientations (shown in *light* and *dark gray*). *F*, solution spectra of CPO measured in the presence or absence of sodium formate and/or ethylene glycol. Measurements were done with solutions containing 0.06 mM CPO in 0.1 M sodium citrate, pH 3.6. Spectra were recorded at 20 °C with a path length of 1 mm using a ND-1000 spectrophotometer (NanoDrop Technologies Inc., Philadelphia, PA).

atom of formate does not occupy the position of the ferric water molecule. However, binding of formate does not leave enough space for the water molecule to bind. The formate molecule forms hydrogen bonds with Glu-183 and an ethylene glycol molecule bound at a similar position as observed in the nitrate structure. Addition of formate to CPO yields a low spin com-

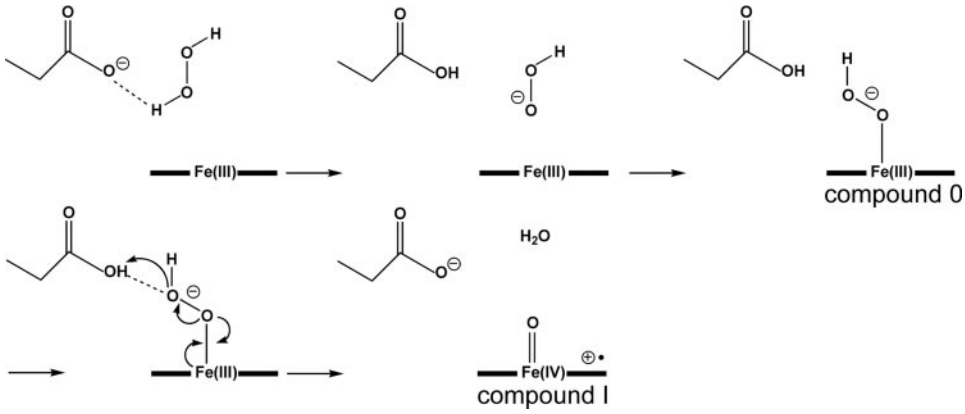

FIGURE 4. **Proposed mechanism of compound I formation catalyzed by chloroperoxidase.**

plex in solution (24), which means that formate binds as the sixth ligand of the heme iron, however, in our structure the distance between the carbon and iron is too long (4.1 Å) for a direct interaction. To evaluate the influence of ethylene glycol on formate binding, we measured solution absorption spectra of CPO in the presence of either formate or ethylene glycol alone, and with both formate and ethylene glycol in a sodium citrate buffer at pH 3.6, comparable to the conditions used for crystallization (Fig. 3*F*). Addition of formate resulted in a Soret band shift from 404 to 424 nm, as expected for the formation of a low spin complex (24). Addition of ethylene glycol (15%) alone caused a small shift of the Soret band to 407 nm. However, when both 100 mM formate and 15% ethylene glycol were added, the Soret peak was at 424 nm, indicating that in solution and at room temperature, addition of ethylene glycol has no influence on formate binding to CPO.

To exclude any influence of ethylene glycol on formate complex formation in the crystal, we also determined the structure of the CPO-formate complex with a sugar-containing cryoprotectant. In this structure (1.6-Å resolution, Fig. 3*E*) the formate binds in two conformations, the first is similar to the one observed in the ethylene glycol-formate complex. But in the sugar structure, this formate forms hydrogen bonds to a water and Glu-183. In the second conformation, the formate molecule binds in a perpendicular orientation above the heme. In this orientation, the formate is a ligand of the heme iron, because the distance between formate oxygen and iron is only 2.1 Å. In contrast to the spectroscopic data, which show the formation of a low spin complex, our crystal structure indicates a mixed spin state of the formate complex similar to the acetate complex structure. This could be a temperature effect because the diffraction data were collected at 100 K, whereas the solution spectra were recorded at room temperature. It has previously been observed that temperature changes can affect the heme spin state (40, 41).

DISCUSSION

We determined the crystal structures of CPO complexed with its substrates and with small ligands, including nitrate, acetate, and formate. Only binding of CPD and acetate induced minor conformational changes at the active site. The side chain of Phe-103 moved 0.5 Å away from the active site to make room for the binding of those compounds. In all structures described here and the previously published complexes of CPO with diatomic or triatomic ligands (23), the catalytic Glu-183 does not undergo conformational changes. The side chain of Glu-183 is "locked," because it forms hydrogen bonds to a water molecule, which also interacts with the propionate group of the heme, and a second hydrogen bond with His-105 (Fig. 2*D*). The carboxylate group of Glu-183 is further stabilized by π-π interactions with heme. Another indicator for the immobility of the Glu-183 side chain is that the side-chain atoms have comparable B-factors with the main-chain atoms in proximity of this residue. It has been proposed that Glu-183, His-105, and Asp-106 function together as a proton relay shuttle facilitating cleavage of H_2O_2 (11, 13).

If one assumes that hydrogen peroxide, the substrate of CPO, binds at the heme in a similar orientation as cyanide, Glu-183 cannot abstract a proton from the proximal oxygen atom bound to the iron (which would correspond to the position of the cyanide carbon) because the distance (3.6 Å) is too long (Fig. 2*D*). Molecular dynamics simulations of a CPO-hydrogen peroxide complex yielded a distance of ~2.5 Å between the proximal oxygen and iron (42). In this case, the distance between the proximal oxygen and deprotonated oxygen of Glu-183 would be 3.3 Å, which is still too long to allow for efficient proton abstraction by Glu-183. Therefore, we conclude that Glu-183 is not capable of catalyzing a 1,2-proton shift required for heterolytic O–O cleavage of a heme-bound hydrogen peroxide molecule.

Based on the structures presented here we propose a new mechanism for H_2O_2 binding to the heme in CPO (Fig. 4). We suggest that the deprotonated Glu-183 first abstracts a proton from the incoming hydrogen peroxide. The generated hydroperoxo-anion then binds at the heme yielding the ferric-hydroperoxo species, compound 0. In the next step, Glu-183 protonates the distal oxygen of compound 0 and the O–O bond is cleaved, water is released, and compound I forms, similar to the Poulos-Kraut mechanism for peroxidases (43–45).

Observation of compound 0 was reported during the reaction of horseradish peroxidase with various peroxides from stopped flow experiments at low temperature, *i.e.* −16 °C or less (46). However, I. Morishima and colleagues could not observe the horseradish peroxidase compound 0 intermediate at ambient temperature with a microsecond-resolved absorption spectrometer (47), although resonance Raman evidence for an Fe–OOH fragment in peroxo-bound myoglobin has in fact been reported (34). Difficulty in detecting the compound 0 species might be due to the fact that the substrate hydrogen peroxide already carries the two protons required for catalysis and that the subsequent heterolytic O–O bond cleavage is rapidly catalyzed by the enzyme, forming compound I.

Compound I reacts with a halide anion to form the hypohalite intermediate. Based on the iodide- and bromide-CPO complexes we suggest that access of halides to the heme is likely to occur through the narrow channel connecting the heme with the surface, although we cannot exclude diffusion via the wide channel. Halide binding sites were identified at the surface close to the narrow channel, within the channel, and at the other end of the narrow channel above the heme.

The iodide-specific binding site above the heme is also a binding site for other polar compounds, including the substrate Me_2SO, acetate, and ethylene glycol. This binding site might act as an intermediate stopping site, possibly orienting the substrate on the path to the heme. Binding at this position is favorable because Asn-74 forms hydrogen bonds with these polar compounds. Polar moieties of larger substrates could also interact with Asn-74. Mutating this residue might affect the stereoselectivity of CPO-catalyzed halogenation and epoxidation/sulfoxidation reactions. We speculate that the stereoselectivity of these reactions might be altered by mutation of Asn-74 to an aliphatic residue (*e.g.* Leu), and Val-182, located on the opposite side of the wide channel, could be changed to Asn or Gln.

CPO has been extensively characterized during the last four decades by biochemical, kinetic, and spectroscopic studies. Here we present crystal structures of CPO complexed with small ligands and its substrates, including the first examples of bound organic compounds, and discuss the implications for compound 0 and compound I formation. For the future it is hoped that crystallographic structure determination of the short-lived reaction intermediates will help to gain a better understanding of the catalytic mechanism of this enzyme.

Acknowledgments—We thank Roger S. Goody for his hospitality, Ingrid Vetter for support of the crystallographic software, and the beamline staff of the Swiss Light Source and European Synchrotron Radiation Facility for their help during data collection.

REFERENCES

1. Beckwith, J. R., and Hager, L. P. (1963) *J. Biol. Chem.* **238,** 3091–3094
2. Beckwith, J. R., Clark, R., and Hager, L. P. (1963) *J. Biol. Chem.* **238,** 3086–3090
3. Hager, L. P., Morris, D. R., Brown, F. S., and Eberwein, H. (1966) *J. Biol. Chem.* **241,** 1769–1777
4. Patterson, E. L., Andres, W. W., and Mitscher, L. A. (1967) *Appl. Microbiol.* **15,** 528–530
5. Itoh, N., Izumi, Y., and Yamada, H. (1987) *Biochemistry* **26,** 282–289
6. Thomas, J. A., Morris, D. R., and Hager, L. P. (1970) *J. Biol. Chem.* **245,** 3129–3134
7. Casella, L., Poli, S., Gullotti, M., Selvaggini, C., Beringhelli, T., and Marchesini, A. (1994) *Biochemistry* **33,** 6377–6386
8. Griffin, B. (1991) in *Peroxidases in Chemistry and Biology* (Everse, J., Everse, K. E., and Grisham, M. B., eds) Vol. II, pp. 85–137, CRC Press, Boca Raton, FL
9. Allain, E. J., Hager, L. P., Deng, L., and Jacobsen, E. N. (1993) *J. Am. Chem. Soc.* **115,** 4415–4416
10. Colonna, S., Gaggero, N., Casella, L., Carrea, G., and Pasta, P. (1993) *Tetrahedron-Asymmetry* **4,** 1325–1330
11. Sundaramoorthy, M., Terner, J., and Poulos, T. L. (1995) *Structure* **3,** 1367–1377
12. Yi, X., Conesa, A., Punt, P. J., and Hager, L. P. (2003) *J. Biol. Chem.* **278,** 13855–13859
13. Wagenknecht, H. A., and Woggon, W. D. (1997) *Chem. Biol.* **4,** 367–372
14. Libby, R. D., Thomas, J. A., Kaiser, L. W., and Hager, L. P. (1982) *J. Biol. Chem.* **257,** 5030–5037
15. Libby, R. D., Beachy, T. M., and Phipps, A. K. (1996) *J. Biol. Chem.* **271,** 21820–21827
16. Griffin, B. W. (1983) *Biochem. Biophys. Res. Commun.* **116,** 873–879
17. Ramakrishnan, K., Oppenhuizen, M. E., Saunders, S., and Fisher, J. (1983) *Biochemistry* **22,** 3271–3277
18. Liu, K. K. C., and Wong, C. H. (1992) *J. Org. Chem.* **57,** 3748–3750
19. Neidleman, S. L., Diassi, P. A., Junta, B., Palmere, R. M., and Pan, S. C. (1966) *Tetrahedron Lett.* **44,** 5337–5342
20. Levine, S. D., Neidleman, S. L., and Oberc, M. (1968) *Tetrahedron* **24,** 2979–2984
21. Colonna, S., Gaggero, N., Manfredi, A., Casella, L., Gullotti, M., Carrea, G., and Pasta, P. (1990) *Biochemistry* **29,** 10465–10468
22. Wang, X., and Goff, H. M. (1997) *Biochim. Biophys. Acta* **1339,** 88–96
23. Sundaramoorthy, M., Terner, J., and Poulos, T. L. (1998) *Chem. Biol.* **5,** 461–473
24. Sono, M., Dawson, J. H., Hall, K., and Hager, L. P. (1986) *Biochemistry* **25,** 347–356
25. Blanke, S. R., Yi, S., and Hager, L. P. (1989) *Biotechnol. Lett.* **11,** 769–774
26. Kabsch, W. (1993) *J. Appl. Crystallogr.* **26,** 795–800
27. Navaza, J. (2001) *Acta Crystallogr. D Biol. Crystallogr.* **57,** 1367–1372
28. Jones, T. A., Zou, J. Y., Cowan, S. W., and Kjeldgaard (1991) *Acta Crystallogr. A* **47,** 110–119
29. Brunger, A. T., Adams, P. D., Clore, G. M., DeLano, W. L., Gros, P., Grosse-Kunstleve, R. W., Jiang, J. S., Kuszewski, J., Nilges, M., Pannu, N. S., Read, R. J., Rice, L. M., Simonson, T., and Warren, G. L. (1998) *Acta Crystallogr. D Biol. Crystallogr.* **54,** 905–921
30. Murshudov, G. N., Vagin, A. A., Lebedev, A., Wilson, K. S., and Dodson, E. J. (1999) *Acta Crystallogr. D Biol. Crystallogr.* **55,** 247–255
31. Perrakis, A., Morris, R., and Lamzin, V. S. (1999) *Nat. Struct. Biol.* **6,** 458–463
32. Kraulis, P. J. (1991) *J. Appl. Crystallogr.* **24,** 946–950
33. Esnouf, R. M. (1999) *Acta Crystallogr. D Biol. Crystallogr.* **55,** 938–940
34. Ibrahim, M., Denisov, I. G., Makris, T. M., Kincaid, J. R., and Sligar, S. G. (2003) *J. Am. Chem. Soc.* **125,** 13714–13718
35. Dauter, Z., Dauter, M., and Rajashankar, K. R. (2000) *Acta Crystallogr. D Biol. Crystallogr.* **56,** 232–237
36. Fedorov, R., Ghosh, D. K., and Schlichting, I. (2003) *Arch. Biochem. Biophys.* **409,** 25–31
37. Blair-Johnson, M., Fiedler, T., and Fenna, R. (2001) *Biochemistry* **40,** 13990–13997
38. Geigert, J., DeWitt, S. K., Neidleman, S. L., Lee, G., Dalietos, D. J., and Moreland, M. (1983) *Biochem. Biophys. Res. Commun.* **116,** 82–85
39. Carlsson, G. H., Nicholls, P., Svistunenko, D., Berglund, G. I., and Hajdu, J. (2005) *Biochemistry* **44,** 635–642
40. Howes, B. D., Feis, A., Indiani, C., Marzocchi, M. P., and Smulevich, G. (2000) *J. Biol. Inorg. Chem.* **5,** 227–235
41. Indiani, C., Feis, A., Howes, B. D., Marzocchi, M. P., and Smulevich, G. (2000) *J. Inorg. Biochem.* **79,** 269–274
42. Filizola, M., and Loew, G. H. (2000) *J. Am. Chem. Soc.* **122,** 3599–3605
43. Poulos, T. L., and Kraut, J. (1980) *J. Biol. Chem.* **255,** 8199–8205
44. Redaelli, C., Monzani, E., Santagostini, L., Casella, L., Sanangelantoni, A. M., Pierattelli, R., and Banci, L. (2002) *Chembiochemistry* **3,** 226–233
45. Rodriguez-Lopez, J. N., Lowe, D. J., Hernandez-Ruiz, J., Hiner, A. N., Garcia-Canovas, F., and Thorneley, R. N. (2001) *J. Am. Chem. Soc.* **123,** 11838–11847
46. Baek, H. K., and Van Wart, H. E. (1992) *J. Am. Chem. Soc.* **114,** 718–725
47. Shintaku, M., Matsuura, K., Yoshioka, S., Takahashi, S., Ishimori, K., and Morishima, I. (2005) *J. Biol. Chem.* **280,** 40934–40938